WOOD RESEARCH **doi.org/10.37763/wr.1336-4561/71.3.505517**
e-ISSN 2729-8906
71(3): 2026 505-517 pp.

THE STUDY ON THE FREQUENCY RESPONSE CHARACTERISTICS OF WOOD ORTHOTROPY BASED ON STRESS WAVE PROPAGATION DIRECTION AND DISTANCE

XINGYU SHAO[1], MING LI[2], SAIYIN FANG[1], TINGTING DENG[1], KUN DU[1], JINGGUI WANG[1], WENTAO XU[1], HAO SHI[1]
[1]SOUTHWEST FORESTRY UNIVERSITY, YUNNAN, CHINA
[2]ANHUI POLYTECHNIC UNIVERSITY, ANHUI, CHINA

(RECEIVED AUGUST 2026)

ABSTRACT

This study investigates the frequency response of *Zelkova schneideriana* and *Pinus sylvestris* var. *mongholica* Litv. along longitudinal, radial, and tangential directions at different propagation distances. Sinusoidal signals from 20 to 200 kHz with 2 kHz intervals were applied using a piezoelectric device, and the responses were recorded by an acoustic emission sensor. Frequency response curves were obtained from the amplitude ratios of response to excitation signals. The results showed that attenuation in the radial direction was lower than that in the longitudinal and tangential directions between 20 and 100 kHz. Both species exhibited stable characteristic response bands around 35, 154, and 188 kHz, which showed good agreement with one-dimensional elastic wave theory, with a minimum relative error of 0.48%. *Zelkova schneideriana* also exhibited a characteristic frequency near 79 kHz and more stable high-frequency responses.

KEYWORDS: Frequency response, natural frequency, orthotropy, stress wave, wood.

INTRODUCTION

Wood is a natural anisotropic biomass material whose acoustic response is strongly influenced by its hierarchical structure and anatomical orientation. Previous studies have mainly focused on the audible range (20 Hz–20 kHz), particularly in musical acoustics. Ahmed et al. (2018) investigated the response of different woods under varying humidity. Zhang et al. (2021) examined relationships among annual-ring width, earlywood ratio, and acoustic elastic properties using ultrasonic methods. Shepherd (2016) studied the low-frequency response of wood used as a primitive guitar. Beyond the audible range, ultrasonic and Acoustic Emission (AE) techniques have been used to evaluate wood defects and mechanical properties. AE is particularly useful as a passive, non-invasive, and non-destructive method. Fang et al. (2017) demonstrated the sensitivity of high-frequency stress waves to internal voids. Guo et al. (2011) identified shifts in characteristic frequency bands during failure of wood-based composites.

Wood consists mainly of cellulose, hemicellulose, and lignin, and its viscoelastic structure affects stress-wave propagation. During propagation, AE signals may exhibit harmonics and frequency aliasing (Wan et al. 2021). Wood AE signals can span approximately 20–200 kHz (Li et al. 2019), while viscoelasticity can modify their frequency range and components. Resonance may also occur when excitation approaches the natural frequency of wood. Therefore, stress waves at different frequencies exhibit different propagation characteristics.

Frequency-dependent attenuation and defect sensitivity have been reported. Huang et al. (2022) showed that surface cracks affect the propagation characteristics and energy attenuation of longitudinal AE signals, while Mao et al. (2022) demonstrated that AE attenuation in wood varies with signal frequency. Li et al. (2017) found that responses above 100 kHz undergo considerable viscoelastic energy dissipation, with signals above 150 kHz showing reduced propagation distances, particularly in defective wood. Xu et al. (2023) observed high attenuation in the 30–50 kHz and 150–170 kHz bands, which were effective for detecting hole defects. Ding et al. (2022) found that signals concentrated in 30–55 kHz during linear deformation, whereas 100–130 kHz components appeared during nonlinear deformation and fracture. Chen et al. (2025) further reported that increasing crack depth altered 31.25–62.5 kHz wavelet energy and enhanced signals around 165 kHz. Wang et al. (2010) demonstrated spatial attenuation of stress waves in heterogeneous materials, while Wu et al. (2025) revealed anisotropic AE propagation in wood. However, the combined effects of propagation distance and orthotropic direction on wood frequency response remain insufficiently characterized. Measured frequency variations may reflect not only the source or damage mechanism but also the interaction between anatomical direction and propagation path length, limiting interpretation in wood health monitoring.

To address this issue, this study investigates the effects of wood texture and propagation distance on frequency response. As shown in Fig. 1, specimens in three orthogonal directions were prepared, with propagation distances of 20–60 mm.

Continuous sinusoidal signals from 20 to 200 kHz were applied at 2 kHz intervals, and recorded amplitudes were converted to dB to construct frequency-response curves. The study aims to quantify frequency-response characteristics, identify characteristic frequency regions, and clarify the effects of orthotropic anisotropy and propagation distance to provide a basis for improving the reliability and efficiency of wood health monitoring (Palma & Steiger 2020).

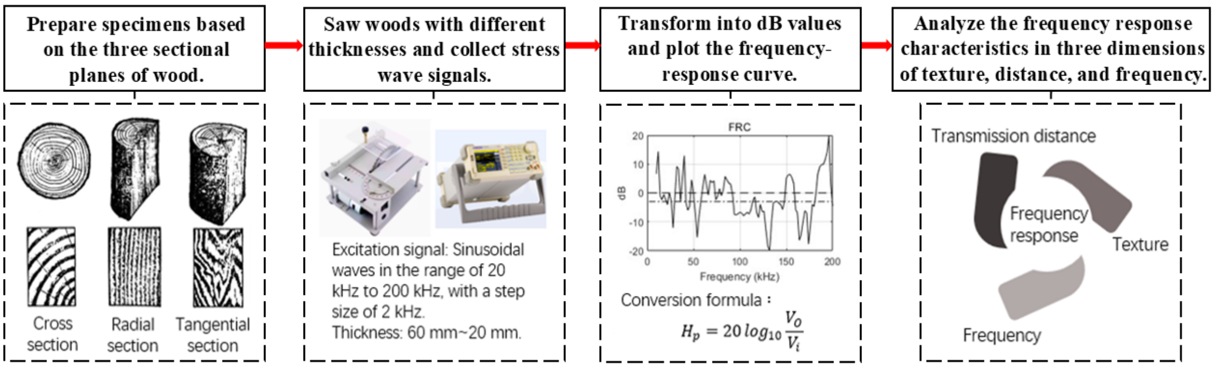

Fig. 1: Schematic diagram of the research process.

MATERIAL AND METHODS

Test equipment

This study employed a single-channel data acquisition system comprising an NI USB-6366 DAQ card and LabVIEW software. A single-ended resonant RS-2A sensor acquired responses within a ±10 V input range. Sampling was performed at 2 MHz, satisfying the Nyquist criterion for faithful signal reconstruction. High-temperature insulating silicone grease coupled the sensor to the wood specimen. Excitation was provided by a SIGLENT SDG805 signal generator (Shenzhen SIGLENT Technology Co., Ltd.), delivering a continuous sine wave from 20 kHz to 200 kHz in 2 kHz steps at 1.5 V output. Each acquisition lasted 2 seconds to ensure stable, steady-state response.

Experimental materials and methods

The study focused on three wood directions: longitudinal, tangential, and radial. We selected air-dried solid wood sawn timber from broad-leaved *Zelkova schneideriana* (T_Z) and *Pinus sylvestris* var. *mongholica* Litv. (T_P) with straight grain and no surface defects (Tab. 1). For each wood species, three specimens were prepared from the same log, corresponding to the three directions of the wood respectively. Each specimen had dimensions of 60 mm × 60 mm × 30 mm. Each specimen was then progressively cut along the stress wave propagation direction to obtain lengths of 50 mm, 40 mm, 30 mm, and 20 mm, and measurements were performed after each cutting step (Fig. 2a).

Tab. 1: Parameters of test materials.

Test specimen	Quantity	Size (mm)	Density (g/cm^3)	Moisture content (%)
T_Z	3	60 × (60~20) × 30	0.615	11.3
T_P	3	60 × (60~20) × 30	0.498	10.8

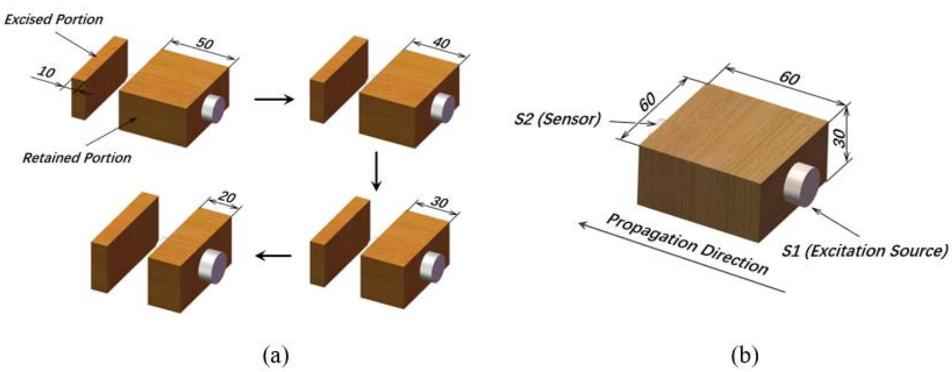

Fig. 2: Diagram of sawn timber cutting (a), diagram of the test setup (b).

Analytical method for the anisotropic frequency response of wood

Sensors S1 and S2 were mounted on the two vertical end faces aligned with the stress-wave propagation direction, both centred on the specimen surface. S1 was connected to the signal generator's output to serve as the excitation source; S2 was placed at the opposite end to receive the propagated signal. This configuration (Fig. 2b) was applied to all specimens across thicknesses. Although the amplitude of the sine signal output by the signal generator is 1.5 V, the amplitude of the actually generated excitation signal varies with the frequency due to the influence of the frequency response characteristics of the S1 sensor. The corresponding excitation signal is:

$$x(t) = A(f)\sin(2\pi ft) \quad (1)$$

where: f is the frequency of the excitation signal, ranging from 20 kHz to 200 kHz, with a 2 kHz change interval, measured in kilohertz.

To address the issue of different amplitudes of excitation sources at different frequencies, this paper uses the decibel value to evaluate the response characteristics. The response amplitude of the excitation signal at the same frequency f_0 passing through specimens of different thicknesses is denoted as A_i, where $i = \{20, 30, 40, 50, 60\}$ (mm). Meanwhile, the response amplitude when the thickness is 20 mm is set as the reference amplitude (Eq. 2). Then the response decibel values at other thicknesses are expressed as Eq. 3:

$$A_r(f_0) = A_{20} \quad (2)$$

$$H_p(f_0) = 20\log_{10}\frac{A_p}{A_r(f_0)}, p \in i, p \neq 20 \quad (3)$$

In the formula, $A_p(f)$ denotes the amplitude of the stress wave signal measured through specimens of thickness 30–60 mm at frequency f; $A_r(f)$ denotes the amplitude measured through a 20 mm specimen. $H_p(f)$ quantifies wood's frequency-dependent gain or attenuation: for example, $H_{40}(f_0) = 15\,dB$ implies $\frac{A_p}{A_r(f_0)} = \frac{A_{40}}{A_{20}} \approx 5.6$, the response amplitude through 40 mm wood is 5.6× that through 20 mm wood at f_0. The −3 dB point defines the cutoff frequency f_c: when $H_p(f) < -3dB$, the signal amplitude drops to 70.7% of its passband maximum, indicating negligible wood response at that frequency. By combining propagation distance with H_p values normalized to peak amplitude, we quantitatively evaluate how stress wave frequency response degrades with distance.

RESULTS AND DISCUSSION

Frequency response analysis of orthotropic wood

The Frequency Response Curve (FRC) characterizes a structure's steady-state dynamic response under excitation and quantifies its amplitude–frequency behaviour (Zhang et al. 2023). This study constructs an anisotropic FRC-based model for wood and analyses its frequency response at key amplitude thresholds-0 dB (unity gain) and −3 dB (cutoff)-across the 20–200 kHz stress wave band. Owing to the anisotropic frequency-dependent attenuation characteristics, frequency ranges were independently delineated for each propagation direction. First, above 60 kHz, specimen TP exhibits pronounced amplitude attenuation with increasing propagation distance. Accordingly, the 20–200 kHz AE frequency band is divided into F_1 (20–60 kHz) and F_2 (60–200 kHz), as shown in Fig. 3.

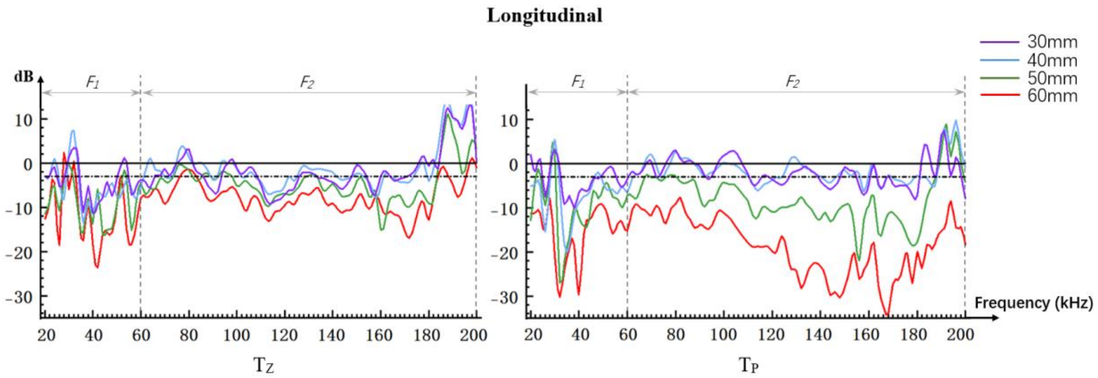

Fig. 3: Longitudinal frequency response curve.

Second, both specimens share common features in their longitudinal-frequency response curves: overall attenuation (−20 to 0 dB) across 20–200 kHz, with three distinct gain peaks at 32±2 kHz, 80±2 kHz, and 186±2 kHz (>0 dB). Specimen T_Z demonstrates superior attenuation resistance compared to T_P-especially above 60 kHz-and yields higher gain values at all three peak frequencies. In contrast, T_P's response curve declines linearly with distance; above 60 kHz, attenuation intensifies, reaching −35±1.5 dB at 166–168 kHz (minimum −35 dB at 166 kHz, corresponding to ~56× amplitude reduction). This stems from uniform viscoelastic dissipation due to aligned wood fibres. Beyond 40 mm, each additional 10 mm incurs ~5±0.5 dB loss; by 60 mm, the entire band falls below 0 dB, and the −3 dB passband vanishes entirely. These findings align with Li et al. (2017), who reported amplitude stratification and severely limited high-frequency transmission over long distances. The T_Z specimen's response remains stable across 60–100 kHz despite increasing propagation distance. Accordingly, the 20–200 kHz band is divided into three sub-bands: F_1 (20–60 kHz), F_2 (60–100 kHz), F_3 (100–200 kHz) (Fig. 4).

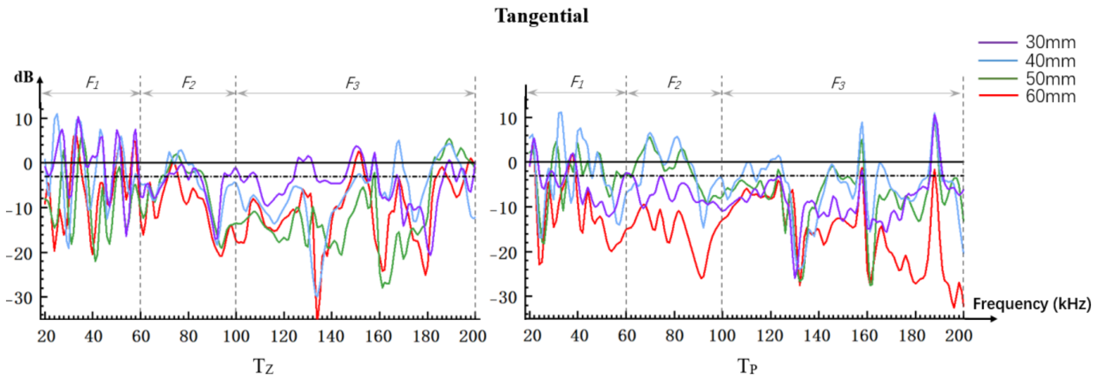

Fig. 4: Tangential frequency response curve.

In F_1 and F_2, both specimens show modest fluctuations (−20 to +10 dB) with distance-indicating weak distance dependence. Notably, T_Z exhibits a resonance peak of +4 dB at 78±2 kHz in F_2, absent in T_P. In contrast, strong attenuation occurs near 136 kHz and 162 kHz: dB values drop to ~−30 dB across all distances, reflecting pronounced anti-resonance (Fan et al. 2025). This stems from tangential grain non-uniformity, which causes multi-path scattering and energy loss-making these frequencies inherently unstable and distance-insensitive. For reliable detection, such anti-resonance bands should be avoided to maintain signal-to-noise ratio. In F_3, responses decline but lack clear trends. However, consistent gain (+5 to +11 dB) appears at 154±2 kHz and 188±2 kHz-identifying them as robust, high-SNR frequency windows for practical use.

Above 100 kHz, the two specimens diverge markedly in stress wave response with increasing propagation distance. Thus, the 20–200 kHz band is split into F_1 (20–100 kHz) and F_2 (100–200 kHz), as shown in Fig. 5. In F_1, TZ consistently outperforms TP: all dB values exceed −3 dB, indicating robust signal transmission. In F_2, only narrow bands at 154±2 kHz and 188±2 kHz remain above −3 dB; elsewhere, both specimens fall below cutoff-confirming strong high-frequency attenuation in wood. Anti-resonance dips occur near 136±1 kHz and 160±2 kHz in the radial direction, but their depth is significantly shallower than in the tangential direction-and only become pronounced beyond 40 mm propagation distance. Within F_2, TZ maintains superior attenuation resistance versus TP. At 40 mm, TZ shows frequency-dependent attenuation, while TP's response declines monotonically and linearly-consistent with its uniform fiber alignment and progressive viscoelastic energy loss. Three consistent gain peaks appear at 32±2 kHz, 154±2 kHz, and 188±2 kHz. At all three, TZ yields higher amplitude: peak ~10±3 dB vs. TP's ~7±3 dB-attributable to TZ's higher density and tighter microstructure, enhancing overall energy retention.

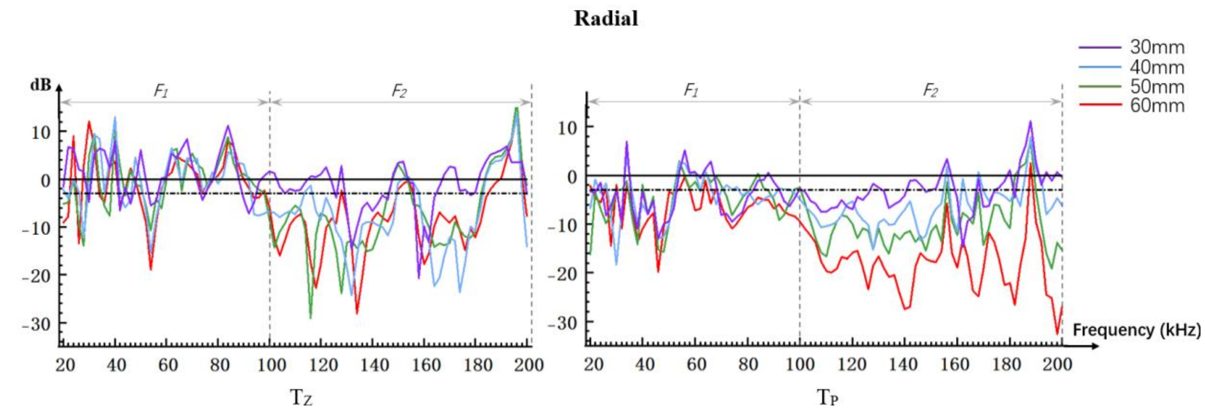

Fig. 5: Radial frequency response curve.

In summary, T_P exhibits linear dB decline with distance in both longitudinal and radial directions-indicating strong distance dependence. In contrast, both T_Z and T_P show their most stable frequency response in the radial direction, with the broadest distance-insensitive frequency band. Overall, propagation distance is a dominant factor: longer paths increase sensitivity to wood's internal structural non-uniformity, degrading signal fidelity.

Due to the significant anisotropy in structural features such as cell morphology, fiber orientation, and ray dimensions, stress wave propagation characteristics of wood differ markedly along the directions. To clarify the influence of grain orientation on frequency response, radial and tangential sections of T_Z and T_P specimens were prepared, stained, and observed under an optical microscope (Leica DM2000, Germany) at 10× magnification to analyse the internal microstructures (Figs. 6–7). Results show that the radial surface exhibits well-developed rays, forming efficient stress wave pathways, resulting in consistently higher dB values compared to the other two directions. In contrast, pores and structural discontinuities in the longitudinal and tangential directions cause scattering and attenuation. The parallel arrangement of fibres in the longitudinal direction leads to uniform accumulation of viscoelastic dissipation over distance, producing nearly linear dB attenuation. Moreover, T_Z has wider rays while T_P displays a more uniform structure-these differences directly explain their distinct frequency responses: T_P shows linear attenuation in the longitudinal direction, whereas T_Z exhibits stronger directional selectivity and nonlinear characteristics.

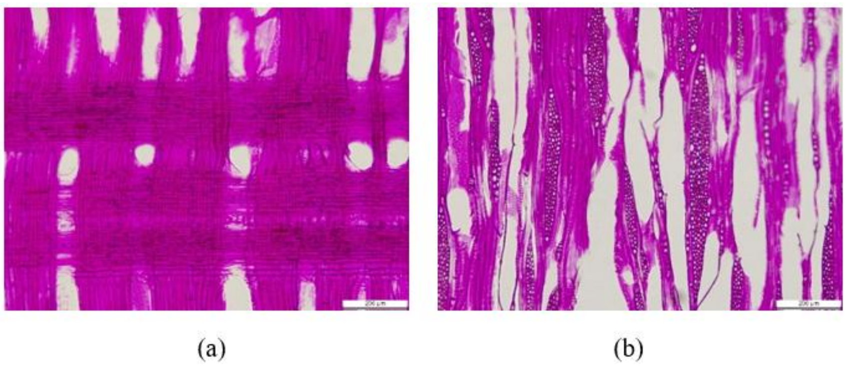

Fig. 6: Microstructure of Zelkova schneideriana wood: (a) radial, (b) of tangential section.

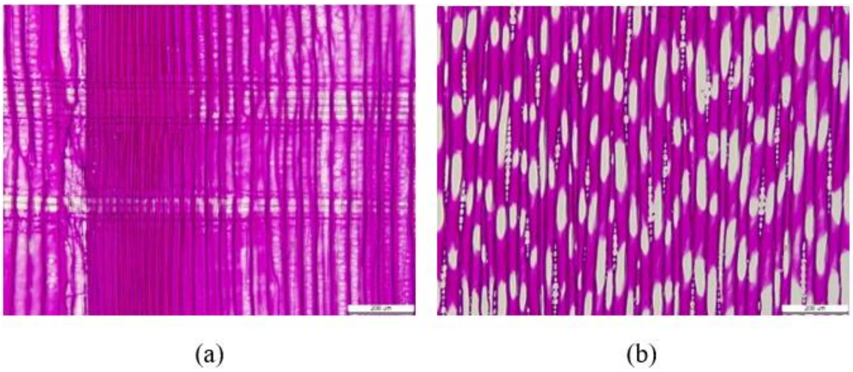

Fig. 7: Microstructure of Pinus sylvestris var. mongholica Litv.: (a) radial section, (b) tangential section.

Analysis of the natural frequency of wood

Wood's natural frequency reflects its elastic modulus, structural integrity, and internal stress-wave propagation behaviour (Guan et al. 2013; Brancheriau & Bailleres 2002). Swept-sine acoustic excitation enables accurate natural frequency estimation (Mituletu et al. 2019). In non-destructive testing, strain energy release excites structural vibration modes, concentrating stress-wave energy in narrow frequency bands (Ding et al. 2021). As confirmed here, and consistent with Hackenberg et al. (2016) and Zhu et al. (2009), resonance peaks occur when excitation frequency matches natural frequency: maximum dB values align precisely with each specimen's natural frequency, indicating clear resonance.

Wood is anisotropic, and grain direction influences its natural frequency. To identify natural frequencies accurately, we extract dominant frequencies-those with prominent, overlapping peaks across the 20-200 kHz band under all three grain directions-and designate them as location-specific significant natural frequencies. For example, Fig. 8 shows the TZ specimen's frequency response at 20 mm and 30 mm propagation distances, revealing significant responses at f_1 = 34 kHz, f_2 = 56 kHz, f_3 = 156 kHz, and f_4 = 188 kHz-indicating likely natural frequencies in this range. Natural frequency bands are then refined by comparing dominant frequencies across all grain directions; results are summarized in Tab 2.

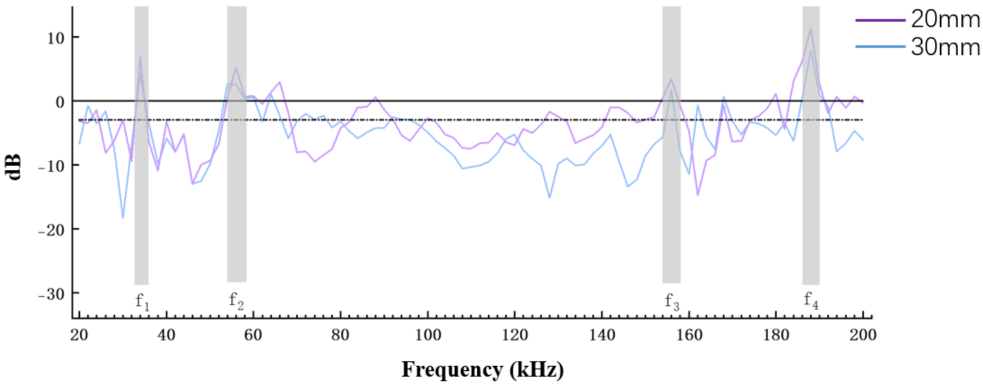

Fig. 8: Frequency response curves of T_Z specimens with propagation distances of 20 mm and 30 mm.

The concentrated frequency bands of each specimen vary little across directions within the experimental frequency range (Tab. 2). However, T_Z specimens exhibit more natural frequency bands than T_P specimens. No directional dependence is observed in TZ specimens, whereas TP specimens show the highest number of natural frequency bands in the radial direction-indicating greater radial-grain stability in frequency response. Frequencies for TZ specimens occur near 35.3, 79.3, 153.3, and 188 kHz; for TP specimens, near 34, 154.7, and 188.7 kHz. These differences reflect how wood density and microstructure influence natural frequency.

Tab. 2: Peak overlapping dominant frequencies of T_Z and T_P specimens.

Texture direction	Specimen	Dominant frequencies (kHz)
Longitudinal	T_Z T_P	34, 80, 152, 188, 198 32, 154, 190
Tangential	T_Z T_P	36, 56, 78, 154, 188 36, 156, 188
Radial	T_Z T_P	36, 48, 80, 154, 188 34, 56, 154, 188

To provide a theoretical baseline for natural frequency extraction, this study models the wood specimen-as oriented along the stress wave path-as a free–free one-dimensional elastic rod. Note that wood is an anisotropic, porous, viscoelastic composite; its actual wave propagation involves boundary effects, internal scattering, damping, and transverse coupling. Thus, this 1D rod model serves not as a predictive tool, but as a first-order approximation to interpret trends in natural frequencies and estimate the approximate location of dominant peaks across grain directions. From the longitudinal wave equation, the nth-mode theoretical natural frequency f_n for a specimen of length L is:

$$f_n = \frac{n}{2L} \cdot c, \mathrm{c} = \left(\sqrt{\frac{E}{\rho}}\right) \tag{4}$$

In this formula, E is the elastic modulus along the propagation direction, ρ is specimen density, and n is the vibration mode $(n = 1, 2, 3 \ldots)$. When excitation frequency f_0 approaches natural frequency f_n, resonance occurs—marked by peak response amplitude. Tensile specimens were prepared following GB/T 1938–2009 ("Test method for tensile strength parallel to grain of wood"), with dumbbell-shaped samples cut from representative locations of both specimen types. Longitudinal elastic modulus was measured using a Shimadzu AG-X 100 kN universal testing machine. Results are reported in Tab. 3; corresponding theoretical longitudinal natural frequencies are listed in Tab. 4.

Tab. 3: Results of the elastic modulus of specimens.

Physical quantity	Unit	T_Z	T_P
Elastic modulus(E)	GPa	12.4	9.4
Wave velocity(c)	m/s	4490.28	4344.59

Tab. 4: Table of theoretical natural frequencies from 1st to 5th order.

L(mm)	Specimen	1st (kHz)	2nd (kHz)	3rd (kHz)	4th (kHz)	5th (kHz)
60	T_Z	37.42	74.84	112.26	149.68	187.10
	T_P	36.21	72.42	108.62	144.84	181.05
50	T_Z	44.90	89.81	134.71	179.61	224.51
	T_P	43.45	86.89	130.34	173.78	217.23
40	T_Z	56.13	112.26	168.39	224.51	280.64
	T_P	54.31	108.62	162.92	217.23	271.54
30	T_Z	74.84	149.68	224.51	299.35	374.19
	T_P	72.41	144.82	217.23	289.64	362.05
20	T_Z	112.26	224.51	336.77	449.03	561.29
	T_P	108.61	217.23	325.84	434.46	543.07

Comparison of Tab. 2 and 4 shows experimental dominant frequencies align closely with theoretical natural frequencies from the 1D elastic wave model under matched geometry. At L = 60 mm, the 1st, 2nd, 4th, and 5th theoretical modes match observed peaks-with TZ's 5th mode differing by just 0.48%. As thickness decreases (e.g., L = 30 mm), experimental peaks shift toward higher-order modes: the 2nd mode (149.68 kHz) aligns with the measured 152 kHz (error = 1.55%). Natural frequency is governed by material stiffness, density, and boundary conditions (Girardi 2021; Ishihara & Noda 2003), representing undamped eigenmodes. Classical theory predicts monotonic increase with decreasing L-but experiments reveal a robust nonlinear pattern: dominant frequencies consistently cluster near three stable bands-35 kHz, 154 kHz, and 188 kHz-regardless of size change. This confirms wood possesses intrinsic, geometry-invariant characteristic frequency bands. The 1D rod model effectively captures the dominant trend of longitudinal stress wave propagation, validating its use for initial natural frequency estimation. However, it cannot replicate wood's full vibrational complexity: real wood is heterogeneous-vessels, lumens, rays, and ring boundaries cause local impedance mismatches-and high-frequency responses involve coupled bending, transverse, and local resonances beyond pure longitudinal motion.

The experimental frequency response peaks align closely with select modes of the 1D rod model-confirming that this simplified theory captures the dominant longitudinal stress wave trend. Yet, dominant frequencies remain stable across specimen sizes, clustering consistently near 35 kHz, 154 kHz, and 188 kHz. This frequency-band stability indicates that peak positions are governed not by classical structural modes alone, but primarily by wood's internal microstructure, wave propagation pathways, and local resonances. Specimen size mainly modulates amplitude and attenuation-not peak location. Thus, these three bands constitute wood's intrinsic characteristic frequencies: they exhibit strong energy concentration, partial correspondence with theoretical modes, and a formation mechanism rooted in material heterogeneity rather than uniform-rod assumptions. These stable, directional bands provide a robust basis for frequency-feature recognition, propagation analysis, and material-state assessment in wood NDT.

CONCLUSIONS

This study investigates how wood anisotropy shapes frequency response under sinusoidal excitation, establishing an anisotropic stress wave frequency response model. Key conclusions are: *(1)* Wood frequency response exhibits strong directionality: longitudinal dB decays linearly with distance; tangential response is highly irregular and disordered; radial response is optimal, frequency bands of 20–100 kHz, 154 kHz, and 188 kHz are nearly unaffected by distance. Overall, T_Z has higher dB values than T_P, with more stable high-frequency attenuation, attributed to its greater density. *(2)* Differences in density and microstructure lead to distinct frequency response characteristics among species: both T_Z and T_P show stable characteristic frequency bands at 35 kHz, 154 kHz, and 188 kHz; additionally, T_Z exhibits a peak at 79 kHz, indicating a more specific high-frequency response. *(3)* Measured dominant peaks closely match the theoretical natural frequencies of a 1D rod across multiple modes (minimum relative error 0.48%), yet the peak positions do not shift significantly with size, suggesting that the dominant mechanism is not governed by classical structural modes but rather by a combination of microstructure, wave propagation paths, and local resonances.

The anisotropic frequency response model developed here establishes a 3D analysis framework, linking frequency, grain direction, and propagation distance, for stress wave detection in wood. It provides experimental support for texture-direction identification, optimal frequency selection, and detection-distance planning in wooden structure health monitoring.

ACKNOWLEDGEMENTS

The authors sincerely appreciate the support from the following projects: Yunnan Agricultural Joint Special Project (202501BD070001-030), National Natural Science Foundation of China (32160345, 31760182), and Yunnan Basic Research Special Project (202201AU070068).

REFERENCES

1. Ahmed, S.A., & Adamopoulos, S. (2018). Acoustic properties of modified wood under different humid conditions and their relevance for musical instruments. *Applied Acoustics*, *140*, 92–99.
2. Brancheriau, L., & Bailleres, H. (2002). Natural vibration analysis of clear wooden beams: A theoretical review. *Wood Science and Technology*, *36*(4), 347–365.
3. Chen, C., Li, M., Fang, S., Zhao, J., Shen, Z., Zhang, Z., & Deng, T. (2025). Study the effect of stress wave energy attenuation characteristics on wood surface cracks based on acoustic emission technology. *Forest Engineering*, *41*(1), 40–49.
4. Ding, R., Luo, R., Fang, S., Lai, F., & Li, M. (2022). Research on wood damage fracture

process based on acoustic emission signal information entropy. *Journal of Northwest Forestry University*, *37*(5), 210–217.

5. Ding, R., Luo, R., & Lai, F. (2021). Straight line location algorithm of wood acoustic emission source based on singular spectrum analysis and signal correlation analysis methods. *Journal of Northwest Forestry University*, *36*(5), 173–178.
6. Fan, Y., Li, H., Li, A., Wang, W., & Wu, Y. (2025). Using antiresonant frequency in the identification of blisk mistuning. *Journal of Aerospace Power*, *40*(4), 18–30.
7. Fang, Y., Lin, L., Lu, Z., & Feng, H. (2017). An air-coupled ultrasonic imaging system for non-destructive wood testing. *Journal of Zhejiang A&F University*, *34*(2), 355–360.
8. Girardi, M. (2021). The natural frequencies of masonry beams. *Archive of Applied Mechanics*, *91*(5), 2369–2379.
9. Guan, X., Zhao, M., Wang, Z., Sha, W., & Zhou, Z. (2013). Research on the stress wave velocity and elastic modulus of poplar logs based on longitudinal resonance method. *Journal of West China Forestry Science*, *42*(2), 14–19.
10. Guo, X., Guo, Y., Hu, W., & Cao, P. (2011). Acoustic emission characterization of wood base composite materials fracture. *Journal of Nanjing Forestry University (Natural Science Edition)*, *35*(3), 97–100.
11. Hackenberg, H.P., & Hartung, A. (2016). An approach for estimating the effect of transient sweep through a resonance. *Journal of Engineering for Gas Turbines and Power*, *138*(082502).
12. Huang, C., Li, M., Fang, S., Zhao, Y.U.E., Mao, F., Yang, Z., & Deng, T. (2022). Research on the effect of wood surface cracks on propagation characteristics and energy attenuation of longitudinal acoustic emission. *Wood Research*, *67*(5), 744–759.
13. Ishihara, M., & Noda, N. (2003). Nonlinear dynamic behavior of a piezothermoelastic laminated plate with anisotropic material properties. *Acta Mechanica*, *166*(1–4), 103–118.
14. Li, X.C., Ju, S., Luo, T. F., & Li, M. (2019). Influence of adhesive layer at Masson pine glulam on acoustic emission signal propagation characteristics. *Journal of Northwest Forestry University*, *34*, 185–190.
15. Li, Y., Luo, T.F., Yu, S.S., Shen, L.J., & Li, M. (2017). Signal propagation characteristics of acoustic emission and Douglas fir glulam beams. *Journal of Northwest Forestry University*, *32*, 197–201.
16. Mao, F., Fang, S., Li, M., Huang, C., Deng, T., Zhao, Y., & Qin, G. (2022). Study on attenuation characteristics of acoustic emission signals with different frequencies in wood. *Sensors*, *22*(16), 5991.
17. Mituletu, I.C., Gillich, G.R., & Maia, N.M. (2019). A method for an accurate estimation of natural frequencies using swept-sine acoustic excitation. *Mechanical Systems and Signal Processing*, *116*, 693–709.
18. Palma, P., & Steiger, R. (2020). Structural health monitoring of timber structures. Review

of available methods and case studies. *Construction and Building Materials*, *248*, 118528.
19. Shepherd, M.R. (2016). Measuring the low-frequency response of an acoustic guitar. *The Journal of the Acoustical Society of America*, *139*(4_Supplement), 2012.
20. Wan, J., Guo, R., Mi, X., Wei, J., & Li, T. (2021). Nonlinear variable parameter time-history analysis of dynamic response of wooden frameworks in Song dynasty palaces and halls. *Journal of Taiyuan University of Technology*, *52*(3), 466–472.
21. Wang, G., Li, C., Hu, S., Feng, C., & Li, S. (2010). A study of time-and spatial-attenuation of stress wave amplitude in rock mass. *Rock and Soil Mechanics*, *31*(11), 3487–3492.
22. Wu, Y., Fang, S., Li, M., Deng, T., Chen, C., & Tian, Z. (2025). Anisotropic propagation characteristics of acoustic emission signals in wood. *Wood Research*, *70*(2), 310–323.
23. Xu, N., Li, M., Fang, S., Huang, C., Chen, C., Zhao, Y., Mao, F., Deng, T., & Wang, Y. (2023). Research on the detection of the hole in wood based on acoustic emission frequency sweeping. *Construction and Building Materials*, *400*, 132761.
24. Zhang, J., Zhang, W., & Zhang, Y.F. (2023). Nonlinear resonant responses of hyperelastic cylindrical shells with initial geometric imperfections. *Chaos, Solitons & Fractals*, *173*, 113709.
25. Zhang, M., Zhang, Q., Li, J., Xu, J., & Zheng, J. (2021). Classification of acoustic emission signals in wood damage and fracture process based on empirical mode decomposition, discrete wavelet transform methods, and selected features. *Journal of Wood Science*, *67*(1), 59.
26. Zhu, X., Cao, J., Wang, F., & Sun, J. (2009). Location nondestructive testing of knot of larch lumber with vibration modal analysis. *Scientia Silvae Sinicae*, *45*(5), 169–172.

XINGYU SHAO, SAIYIN FANG, TINGTING DENG, KUN DU, JINGGUI WANG,
WENTAO XU, HAO SHI
SOUTHWEST FORESTRY UNIVERSITY
SCHOOL OF MACHINERY AND TRANSPORTATION
KUNMING, YUNNAN, CHINA

MING LI*
ANHUI POLYTECHNIC UNIVERSITY
[1]KEY LABORATORY OF ADVANCED PERCEPTION AND INTELLIGENT CONTROL
OF HIGH-END EQUIPMENT OF MINISTRY OF EDUCATION
[2]SCHOOL OF ELECTRICAL ENGINEERING
WUHU, ANHUI, CHINA
*Corresponding author: swfu_lm@swfu.edu.cn